J. Fluid Mech. (2009), *vol.* 623, *pp.* 59–74.
doi:10.1017/S0022112008005211 Printed in the United Kingdom

Three-dimensional instabilities of oscillatory equatorial zonal shear flows

ANDREI NATAROV† AND KELVIN J. RICHARDS

International Pacific Research Center, University of Hawaii at Mānoa, Honolulu, Hawaii

(Received 14 September 2007 and in revised form 6 October 2008)

In this paper, we investigate the linear stability of oscillating zonal flows on the equatorial β-plane in the presence of fully three-dimensional disturbances. To exclude inflection point effects, we focus on the simplest case of a linear meridional shear with time-mean and oscillating components. For purely oscillatory background flows we find that in addition to resonant excitation of 'additive' type that occurs in the zonally invariant case, resonant excitation of 'difference' type is also possible. For flows with an oscillatory shear superimposed on an unstable time-mean shear it is shown that while the oscillatory shear has a stabilizing influence on disturbances with a small zonal wave number k, at higher k the effect of the oscillating shear diminishes and can even be destabilizing. Overall, a small oscillatory shear tends to reduce the fastest growth rate in the system and pushes the dominant k to higher values. Calculation of dominant zonal and vertical modes shows that the zonally asymmetric modes dominate a large portion of the parameter space, especially at high time-mean background shear and low oscillatory shear. As a result, the dominant vertical mode can have a somewhat larger vertical scale than in the zonally invariant case. At intermediate values of the time-mean shear the growth rate is relatively flat with respect to the zonal mode number, with maximum growth rate occurring in bands of high and low k. We have uncovered a rich assortment of vertical and zonal modes which are likely to play a role in the nonlinear evolution of equatorial flows.

1. Introduction

In addition to the familiar barotropic/baroclinic instabilities of a zonal mean flow, equatorial ocean currents are also subject to instabilities that favour much smaller vertical scales of the order of tens of metres but with relatively large meridional and zonal extents. A manifestation of such small vertical scale (SVS) features in the equatorial thermocline is the presence of the interleaving of water masses (see, for example, Richards & Banks 2002; Lee & Richards 2004).

There are a number of ways in which the instability of a 'steady' zonal current with a large vertical scale can account for these SVS features. Any inviscid zonal flow that has a non-zero meridional shear at the equator is unstable to inertial instability (II; e.g. Dunkerton 1981). Apart from II, there exist other types of SVS-favouring instabilities. Taniguchi & Ishiwatari (2006) identified these instabilities as resonances between equatorial Kelvin modes and continuous modes and those between Kelvin modes and westward mixed Rossby–gravity (MRG) modes. The resonances favour zonally asymmetric disturbances.

† Email address for correspondence: natarov@hawaii.edu

Unlike the steady background flows studied in the aforementioned papers, the realistic large vertical scale flows in the equatorial ocean are time-dependent. As well as having a system of vigorous zonal jets with meridional and vertical shears, the upper equatorial ocean is influenced by equatorially trapped waves (Philander 1990). Here we study the stability of zonal equatorial currents that are oscillatory in time. We extend the study of Natarov, Richards & McCreary (2008), in which the attention was confined to zonally symmetric modes, to the analysis of fully three-dimensional disturbances. In § 2 we present the governing equations, their projection onto vertically and zonally propagating waves and the method used to analyse their stability. Sections 3 and 4 deal with the inviscid dynamics of a projection onto a single vertical mode. Our previous work on zonally symmetric instabilities has shown that qualitatively different regimes arise in cases with large steady shear and a small steady shear. We therefore study these two cases separately. Section 3 is focused on the stability of a weak purely oscillatory zonal flow (no time-mean shear), and in § 4 we describe the effect of oscillatory shear on an unstable time-mean shear flow. Section 5 combines the results for different vertical modes and describes dominant vertical and zonal scales in the parameter space of the magnitudes of the time-mean and oscillatory shears. Section 6 presents the summary and discussion.

2. The governing equations

2.1. *Dimensional equations*

Let t denote time and x the zonal (eastward), y the meridional (northward) and z the vertical (upward) coordinates. We consider a zonal flow $U(y,t)$, i.e. zonally uniform, on the equatorial β-plane. The domain is periodic in the zonal (with the length L_x) and vertical (with the height H) directions and extends from $-\infty$ to $+\infty$ in the meridional direction. The background stratification is assumed constant and characterized by the buoyancy frequency N. The linear evolution of a disturbance (u, v, w, ψ, b), where u, v and w are the zonal, meridional and vertical components of velocity respectively, ψ the pressure divided by a reference density ρ_* and b the buoyancy associated with a perturbation, is then governed by the set of equations

$$\left(\frac{\partial}{\partial t} + U\frac{\partial}{\partial x}\right)u + \left(\frac{\partial U}{\partial y} - \beta y\right)v + \frac{\partial \psi}{\partial x} = 0, \tag{2.1a}$$

$$\left(\frac{\partial}{\partial t} + U\frac{\partial}{\partial x}\right)v + \beta y u + \frac{\partial \psi}{\partial y} = 0, \tag{2.1b}$$

$$\frac{\partial \psi}{\partial z} - b = 0, \tag{2.1c}$$

$$\left(\frac{\partial}{\partial t} + U\frac{\partial}{\partial x}\right)b + N^2 w = 0, \tag{2.1d}$$

$$\frac{\partial u}{\partial x} + \frac{\partial v}{\partial y} + \frac{\partial w}{\partial z} = 0, \tag{2.1e}$$

where a hydrostatic balance has been assumed. The boundary conditions are chosen to be periodic in the zonal and vertical directions. Such choice simplifies the analysis without restricting the generality of the approach. In the meridional direction the disturbances are required to decay to zero as $|y| \to \infty$.

Following a standard procedure to reduce the system (2.1) to a set of three prognostic equations, we obtain

$$\frac{\partial w}{\partial z} = -\left(\frac{\partial}{\partial t} + U\frac{\partial}{\partial x}\right)\frac{1}{N^2}\frac{\partial b}{\partial z} \tag{2.2}$$

and

$$\frac{\partial b}{\partial z} = \frac{\partial^2 \psi}{\partial z^2} \tag{2.3}$$

after differentiating (2.1*d*) and (2.1*c*) with respect to z. Combining (2.2) and (2.3) to form

$$\frac{\partial w}{\partial z} = -\left(\frac{\partial}{\partial t} + U\frac{\partial}{\partial x}\right)\frac{1}{N^2}\frac{\partial^2 \psi}{\partial z^2}, \tag{2.4}$$

we substitute the result into the continuity equation (2.1*e*) to obtain a prognostic equation for ψ:

$$\left(\frac{\partial}{\partial t} + U\frac{\partial}{\partial x}\right)\frac{\partial^2 \psi}{\partial z^2} - N^2\left(\frac{\partial u}{\partial x} + \frac{\partial v}{\partial y}\right) = 0. \tag{2.5}$$

The equations (2.1*a*), (2.1*b*) and (2.5) form a system of three prognostic equations.

Taking advantage of the governing equations being homogeneous in x and z, we seek wavelike solutions of the form

$$\phi(x, y, z, t) = \sum_{k,m} \hat{\phi}_{km}(y, t) e^{\mathrm{i}(kx+mz)}, \tag{2.6}$$

where k is the zonal wave number; m is the vertical wave number; and ϕ stands for u, v or ψ. For a particular (k, m) mode we thus obtain

$$\left(\frac{\partial}{\partial t} + \mathrm{i}kU\right)\hat{u}_{km} + \left(\frac{\partial U}{\partial y} - \beta y\right)\hat{v}_{km} + \mathrm{i}k\hat{\psi}_{km} = 0, \tag{2.7a}$$

$$\left(\frac{\partial}{\partial t} + \mathrm{i}kU\right)\hat{v}_{km} + \beta y\hat{u}_{km} + \frac{\partial \hat{\psi}_{km}}{\partial y} = 0, \tag{2.7b}$$

$$\left(\frac{\partial}{\partial t} + \mathrm{i}kU\right)\hat{\psi}_{km} + c_m^2\left(\mathrm{i}k\hat{u}_{km} + \frac{\partial \hat{v}_{km}}{\partial y}\right) = 0, \tag{2.7c}$$

where $c_m^2 = N^2/m^2$.

2.2. *Non-dimensionalized equations*

We next non-dimensionalize the system (2.7) by introducing a characteristic time scale. For the purpose of our study, the natural time scale is provided by the inverse of the equatorial inertial frequency $\omega_{m,\mathrm{i}} = \sqrt{\beta c_m}$ for a given vertical wavenumber m. Since the equatorial inertial frequency determines the equatorial Rossby radius of deformation $R_m = \sqrt{c_m/\beta}$, it also sets a natural horizontal spatial scaling.

In the remainder of this section, we will omit the subscripts k and m that refer to a specific mode. To summarize, the non-dimensionalized independent variables are

$$\tilde{t} = \sqrt{\beta c}\, t, \quad \tilde{x} = \frac{x}{R}, \quad \tilde{y} = \frac{y}{R}. \tag{2.8}$$

After scaling the velocities with c,

$$\{\tilde{U}, \tilde{u}, \tilde{v}\} = \frac{1}{c}\{U, u, v\}, \tag{2.9}$$

and ψ with c^2,

$$\tilde{\psi} = \frac{\psi}{c^2}, \tag{2.10}$$

the set of the governing equations (2.7) becomes (with tildes omitted)

$$\left(\frac{\partial}{\partial t} + \mathrm{i}kU\right)\hat{u} + \left(\frac{\partial U}{\partial y} - y\right)\hat{v} + \mathrm{i}k\hat{\psi} = 0, \tag{2.11a}$$

$$\left(\frac{\partial}{\partial t} + \mathrm{i}kU\right)\hat{v} + y\hat{u} + \frac{\partial \hat{\psi}}{\partial y} = 0, \tag{2.11b}$$

$$\left(\frac{\partial}{\partial t} + \mathrm{i}kU\right)\hat{\psi} + \left(\mathrm{i}k\hat{u} + \frac{\partial \hat{v}}{\partial y}\right) = 0. \tag{2.11c}$$

Apart from the background zonal velocity U, solutions to the system (2.11) only depend on the non-dimensionalized zonal wavenumber k. As in Natarov *et al.* (2008), our choice of the background zonal velocity is

$$U(y,t) = (\bar{\Lambda} + \delta\Lambda\cos\Omega t)y, \tag{2.12}$$

i.e. a combination of a background time-mean shear $\bar{\Lambda}$ and an oscillating shear of magnitude $\delta\Lambda$ and frequency Ω. Notice that all free parameters in the expression for the background velocity (2.12), $\bar{\Lambda}$, $\delta\Lambda$ and Ω, are non-dimensionalized by dividing by the inertial frequency $\sqrt{\beta c}$. The complete sweep of the four-dimensional parameter space $(k, \bar{\Lambda}, \delta\Lambda, \Omega)$ is out of the question, and we therefore have to be selective in our analysis.

2.3. *Floquet analysis*

To perform a numerical stability analysis of the system, the governing equations (2.11) are discretized using finite differencing on a staggered grid in the meridional coordinate y. The grid points for the velocity fields u, v are located in between the points for the pressure ψ. Meridional walls are introduced at the northern and southern boundaries of the computational domain, far enough so as not to unduly influence the results. The appropriate boundary condition in this setting is a no normal flow ($v = 0$) requirement at each wall. Ghost grid points slightly beyond the physical domain have to be introduced for ψ. The values of ψ at the ghost grid points are updated by keeping the zonal flow at the boundaries in geostrophic balance. This sets the meridional velocity tendency $\partial v/\partial t$ to zero at the boundaries.

To find instabilities the resulting system is subjected to a Floquet analysis. Column vectors in the monodromy matrix represent the projections of the fields onto a basis of Hermite functions for each field. The evolution of the monodromy matrix is calculated using a fourth-order Runge–Kutta method. After propagating the monodromy matrix for one period of the background flow oscillation, the eigenvalues and eigenvectors of the resulting Floquet matrix are calculated using an inbuilt MATLAB eigensolver. Meridional resolution of 64 grid points suffices for all the experiments described below, as the results are essentially unchanged by doubling the resolution. Simulations with 66 time steps per forcing period produce essentially the same results as simulations with 1000 time steps per forcing period.

3. Purely oscillatory shear flows

The stability of purely oscillatory flows in the context of the two-dimensional vorticity equation has recently been addressed by Poulin, Flierl & Pedlosky (2003).

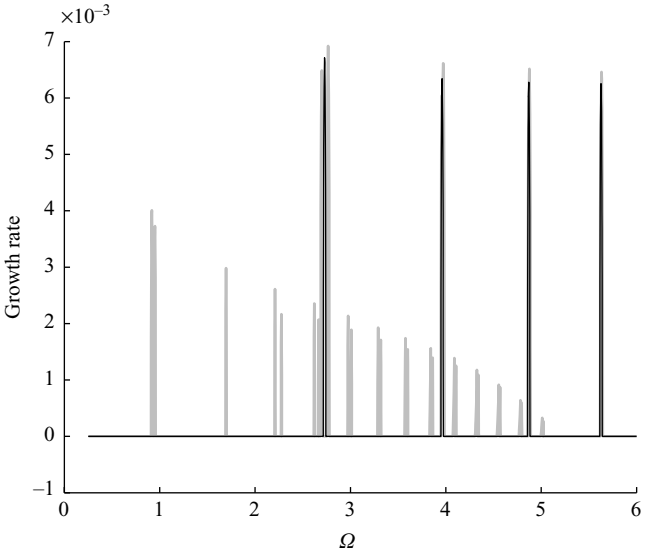

FIGURE 1. The collective growth rate for zonally symmetric ($k=0$) modes (black line) and $k=0.1$ modes (grey lines) as a function of the background frequency Ω. The four black spikes shown correspond to the cases $\Omega=1+\sqrt{3}$, $\Omega=\sqrt{3}+\sqrt{5}$, $\Omega=\sqrt{5}+\sqrt{7}$ and $\Omega=\sqrt{7}+3$. Note grey spikes in the vicinity of the natural frequencies of free equatorial waves at $\Omega=1$, $\sqrt{3}$, $\sqrt{5}$, etc. The magnitude of the oscillatory shear $\delta\Lambda$ is set to 0.05.

One of the interesting findings of that paper is that if the time-periodic background velocity $U(y,t)$ can be represented as a separable function of t and y, as we have here, then the flow is stable. To be unstable, the background zonal velocity has to be comprised of at least two distinct oscillating out of phase profiles.

Our numerical calculations show that in the case of the dynamics studied here such a requirement on the background flow for instability can be relaxed, and we can safely restrict attention to the background flows of the form (2.12). The Poulin *et al.* (2003) results are recovered in the context of our model in the horizontally non-divergent limit $c_m \to \infty$.

Here we set $\bar{\Lambda}=0$, fix $\delta\Lambda$ at a small value of 0.05 and study the changes in the stability of the modes with different k, as we vary the frequency of the background flow oscillation. Along with the dominant disturbance, we also keep track of the next few Floquet vectors. This helps in the interpretation of the changes in the dominant modes throughout the parameter space.

To investigate parametric excitation of the equatorial waves, it is convenient to first revisit the zonally symmetric case $k=0$. The system only possesses a discrete spectrum consisting of frequencies 1 (MRG wave), $\sqrt{3}$, $\sqrt{5}$, etc. (inertia–gravity waves) in this case. Figure 1 shows the collective growth rate of $k=0$ modes as a function of the forcing frequency (thick black curve). The four spikes shown correspond to the cases $\Omega=1+\sqrt{3}$, $\Omega=\sqrt{3}+\sqrt{5}$, $\Omega=\sqrt{5}+\sqrt{7}$ and $\Omega=\sqrt{7}+3$. This is consistent with the multiple-scale analysis of d'Orgeville & Hua (2005), who found that a small linear oscillating shear will *only* excite modes with adjacent meridional mode numbers, whose natural frequencies add up to the frequency of the background flow oscillation. With a non-zero k the spectrum of waves is considerably richer. Corresponding to each meridional mode $\ell > 0$, there now exist two gravity waves and a Rossby wave, all with

distinct frequencies. The MRG waves (with $\ell = 0$) acquire two distinct frequencies as the zonal symmetry is relaxed. In addition, for each k there is now an equatorial Kelvin wave. The grey curve in figure 1 shows the growth rate as a function of Ω for a small value of k ($= 0.1$). While the frequencies of the waves are not substantially altered by such a small k, we can clearly see a dramatic difference in the stability of the system. A large number of additional spikes appear. In particular, unlike in the zonally symmetric case, the background flow oscillations are now capable of exciting destabilizing waves that have frequencies close to the background frequency Ω, i.e. at $\Omega \approx 1, \sqrt{3}, \sqrt{5}$, etc. The idea that first comes to mind is that these new instabilities are due to the interaction of these waves with Kelvin or Rossby waves, which have small frequencies at small k.

To test this conjecture we compare the meridional structure of the unstable Floquet vectors for the $\Omega = 1 + \sqrt{3}$ spike in a zonally symmetric case, the same spike but for $k = 0.1$ and the new spike for $k = 0.1$ that is located close to $\Omega = 1$ which has no counterpart in a zonally symmetric case. The meridional structure of the dominant disturbance in the zonally symmetric case was first calculated by d'Orgeville & Hua (2005). The structure of the perturbation meridional component of velocity $\hat{v}$ of the unstable disturbance at $\Omega = 1 + \sqrt{3}$ is a superposition of the zeroth and first Hermite functions. There are two Floquet vectors corresponding to this mode, with similar meridional structure but with complex conjugate growth rates. These correspond to an upward-propagating and a downward-propagating disturbance.

For $\Omega \approx 1 + \sqrt{3}$ and small k there are now two spikes of similar magnitude in the vicinity of the background frequency, corresponding to the first two fastest growing Floquet vectors, due to the asymmetry between westward- and eastward-propagating waves. Together with slightly different frequencies, the unstable disturbances exhibit slightly different growth rates. However, the meridional structure of the dominant disturbances is very similar to that in the zonally symmetric case.

Finally, for $\Omega \approx 1$ and small k, the first two fastest growing Floquet vectors no longer have similar growth rates. Instead, the fastest growing Floquet vector has a meridional structure comprised mostly of a projection on the MRG wave but with a noticeable projection on the equatorial Kelvin wave as well. The second fastest Floquet vector has a much smaller growth rate and projects almost exclusively onto the equatorial Kelvin wave, with some contribution from the MRG wave. The above conjecture therefore holds.

If we assume that the zonally asymmetric instabilities must satisfy the same resonant combination of 'additive' type ($\Omega = |\omega'| + |\omega''|$), as the zonally symmetric instabilities, then there still remain unexplained spikes in figure 1. For example, a spike around $\Omega \approx 0.9$ cannot be explained by any resonant combination of additive type, as the frequencies of the gravity waves (including the MRG wave) are larger than 0.9. The non-dimensional frequencies of the Rossby waves and the Kelvin wave are approximately equal to $|k|$ for small k and are too small to add up to 0.9 in a low-order interaction. This motivates the question as to whether these spikes can be explained by appeal to resonant combinations of the 'difference' type ($\Omega = |\omega'| - |\omega''|$). For example, the spikes that are very close to the natural frequencies of the normal modes (such as around $\Omega = 1$) on a closer examination are located at frequencies slightly smaller than the natural frequencies. They can be accounted for by resonant combinations of difference type between a gravity wave (or an MRG wave) and a Rossby or the Kelvin wave, which have very small frequencies at small k. But why do such resonances, of difference type, only occur in the zonally asymmetric case?

And what determines the growth rates and the stability boundaries? To answer these questions we turn to a multiple-scale analysis.

3.1. *Multiple-scale analysis*

It is convenient to rewrite the governing system (2.11) for a fixed k and m in the form of a Schrödinger equation:

$$\mathrm{i}\frac{\partial}{\partial t}|\phi\rangle = (\mathscr{H}_0 + \delta\Lambda\mathscr{H}_1\cos\Omega t)\,|\phi\rangle\,, \tag{3.1}$$

where $|\phi\rangle$ is a representation of the solution $[\hat{u}, \hat{v}, \hat{\psi}]^T(y,t)$ and $\mathscr{H}_0$ and $\mathscr{H}_1$ are the linear operators describing the steady and the oscillatory parts of the equation, respectively.

It is convenient to select a representation in which an arbitrary disturbance can be represented as a series expansion in terms of the eigenvectors of the operator $\mathscr{H}_0$:

$$\mathscr{H}_0\,|j\rangle = \omega_j\,|j\rangle\,, \tag{3.2}$$

where j ranges over the index set

$$\{K, M^-, M^+, R_1, G_1^-, G_1^+, \ldots, R_\ell, G_\ell^-, G_\ell^+, \ldots\}, \tag{3.3}$$

where K corresponds to the Kelvin wave, M^- and M^+ to the westward and eastward MRG waves respectively, R_ℓ to the meridional-mode-ℓ Rossby wave and G_ℓ^- and G_ℓ^+ to the westward and eastward meridional-mode-ℓ gravity waves respectively. Note that since we are confining ourselves to positive zonal wavenumbers k, the frequencies ω_j of westward-propagating waves are negative. The eigenvectors $|j\rangle$ encode the meridional structure of the fields corresponding to the given equatorial wave j and are functions of y only (see the Appendix for explicit expressions).

The completeness of waves (3.3) on an equatorial β-plane is well established (e.g. Ripa 1982). Therefore any evolving disturbance $|\phi\rangle$ can be represented as

$$|\phi\rangle\,(y,t) = \sum_j \alpha_j(t)\,|j\rangle\,(y). \tag{3.4}$$

Substituting the expansion (3.4) into the Schrödinger equation (3.1) results in a system of ordinary differential equations (ODEs):

$$\mathrm{i}\frac{\mathrm{d}}{\mathrm{d}t}\alpha_j = \omega_j\alpha_j + \delta\Lambda\cos\Omega t\sum_n \gamma_{jn}\alpha_n, \tag{3.5}$$

where

$$\gamma_{jn} = \langle j|\,\mathscr{H}_1\,|n\rangle\,. \tag{3.6}$$

Thus, the only inputs from our β-plane model needed for further analysis are the spectrum of $\mathscr{H}_0$ and the coefficients γ_{jn}. Both are calculated and described in the Appendix.

The system (3.5) can be further simplified by substituting

$$\alpha_j(t) = A_j(t)\mathrm{e}^{-\mathrm{i}\omega_j t}. \tag{3.7}$$

The resulting governing equation for A_j is

$$\mathrm{i}\frac{\mathrm{d}}{\mathrm{d}t}A_j = \delta\Lambda\cos\Omega t\sum_n \gamma_{jn}A_n\exp[\mathrm{i}t(\omega_j - \omega_n)]. \tag{3.8}$$

Since $\cos \Omega t = (e^{i\Omega t} + e^{-i\Omega t})/2$, (3.8) can be rewritten as

$$i\frac{d}{dt}A_j = \frac{\delta\Lambda}{2}\sum_n \gamma_{jn}A_n\{\exp[it(\omega_j - \omega_n + \Omega)] + \exp[it(\omega_j - \omega_n - \Omega)]\}. \tag{3.9}$$

Assuming $\delta\Lambda \ll 1$, we introduce a slow time $T = \delta\Lambda t$ and a fast time $\tau = t$ and replace the time derivative d/dt with $\partial/\partial\tau + \delta\Lambda\partial/\partial T$ in the governing equation (3.5). We seek asymptotic solutions

$$A_j(t;\delta\Lambda) \sim A_j(\tau, T;\delta\Lambda) \sim A_j^0(T) + \delta\Lambda A_j^1(\tau, T) + O(\delta\Lambda^2). \tag{3.10}$$

The zeroth-order $O(\delta\Lambda^0)$ equations are trivially satisfied, and at the first order $O(\delta\Lambda)$ we have

$$i\frac{\partial}{\partial\tau}A_j^1 = -i\frac{dA_n^0}{dT} - \frac{1}{2}\sum_n \gamma_{jn}A_n^0\left(e^{i(\Omega+\omega_j-\omega_n)\tau} + e^{i(-\Omega+\omega_j-\omega_n)\tau}\right). \tag{3.11}$$

The terms that may contribute to the secular forcing on the right-hand side of (3.11) are those for which $\Omega + \omega_j - \omega_n = 0$ or $-\Omega + \omega_j - \omega_n = 0$. Thus, a given wave j may potentially be destabilized by two waves n_1 and n_2, one with $\omega_{n_1} = \omega_j + \Omega$ and the other with $\omega_{n_2} = \omega_j - \Omega$. While it is possible for some rare combinations of parameters for n_1 and n_2 waves to occur simultaneously, in general only one of these waves will be involved in the resonance with the wave j. We will therefore focus on the two-wave excitations. Notice that ω_j and ω_n always enter the resonance condition multiplied by opposite signs. Thus, resonances of 'additive' type correspond to the case in which ω_j and ω_n have opposite signs, while resonances of 'difference' type correspond to the case in which ω_j and ω_n have the same sign. Assume that $\omega_j - \omega_n - \Omega = 0$. Then $\omega_n - \omega_j + \Omega = 0$, and the amplitudes of the waves j and n are governed by

$$i\frac{dA_j^0}{dT} = \frac{1}{2}\gamma_{jn}A_n^0, \tag{3.12a}$$

$$i\frac{dA_n^0}{dT} = \frac{1}{2}\gamma_{nj}A_j^0. \tag{3.12b}$$

Combining the two first-order equations (3.12a, b) into one second-order equation yields

$$\frac{d^2A_j^0}{dT^2} + \frac{1}{4}\gamma_{jn}\gamma_{nj}A_j^0 = 0. \tag{3.13}$$

The behaviour of the system depends on the sign of $\gamma_{jn}\gamma_{nj}$. If $\gamma_{jn}\gamma_{nj}$ is negative then there is exponential growth at the rate given by

$$\sigma = \sqrt{-\gamma_{jn}\gamma_{nj}}/2. \tag{3.14}$$

If $\gamma_{jn}\gamma_{nj}$ is positive, the wave amplitudes will slowly vacillate with the frequency $\sqrt{\gamma_{jn}\gamma_{nj}}/2$.

For zonally symmetric waves it can be shown that the instability condition $\gamma_{jn}\gamma_{nj} < 0$ can only be satisfied by waves with frequencies of opposite signs. Therefore, only resonances of additive type are possible. One may conjecture that when the amplitude of the background flow oscillation is large enough, the resonances of difference type may occur in the zonally symmetric case as well, through parametric instability of the amplitude equation (3.13). Our numerical calculations show that this is indeed the case.

Ω	Pair	σ_{ms}, 10^{-3}	σ_{num}, 10^{-3}
0.92	$\{M^-, R_1\}$	4.02	4.01
0.95	$\{K, M^+\}$	3.74	3.73
1.70	$\{G_1^-, R_2\}$	2.99	2.98
2.21	$\{G_2^-, R_3\}$	2.62	2.61
2.28	$\{R_1, G_2^+\}$	2.21	2.17
2.62	$\{G_3^-, R_4\}$	2.41	2.36
2.67	$\{R_2, G_3^+\}$	2.18	2.07
2.70	$\{M^-, G_1^+\}$	6.49	6.49
2.77	$\{M^+, G_1^-\}$	6.93	6.92
2.98	$\{G_4^-, R_5\}$	2.26	2.14
3.02	$\{R_3, G_4^+\}$	2.11	1.89
	...		

TABLE 1. Forcing frequency Ω at which instability occurs, pairs of waves excited, and growth rates from the multiple scales calculations, σ_{ms}, and numerical Floquet analysis, σ_{num}.

Parameter	Value	Interpretation
β	$2.29 \times 10^{-11}\,\mathrm{m^{-1}\,s^{-1}}$	gradient of Coriolis parameter
N	$0.015\,\mathrm{s^{-1}}$	background buoyancy frequency
g	$9.78\,\mathrm{ms^{-2}}$	gravitational acceleration
ρ_*	$1020\,\mathrm{kg\,m^{-3}}$	reference density
T	22 days	forcing period
L_x	14, 443 km	domain length in zonal direction
L_y	500 km	domain meridional half-width
H	200 m	domain height
ν	$10^{-6}\,\mathrm{m^2\,s^{-1}}$	vertical viscosity

TABLE 2. The parameters for the dimensional model.

As an example of a zonally asymmetric case, we consider an interaction of a Kelvin wave with an MRG wave. It can be shown that

$$\gamma_{KM}\,\gamma_{MK} = -k\frac{\omega_M}{|\omega_M|}\frac{1}{2}\frac{\sqrt{1-s_M}}{2-s_M} \tag{3.15}$$

(see the Appendix for notation). Instability occurs if $\omega_M > 0$. Since $\omega_K > 0$, this instability corresponds to a resonance of difference type. This supports our conjecture that resonances of difference type as well as resonances of additive type occur in the zonally asymmetric case. The explicit algebraic expressions for other combinations of waves can be easily derived from the equations given in the Appendix by specifying the types of waves. Table 1 summarizes the results for the first few peaks by showing the growth rate σ_{ms} given by (3.14) and excited wave pairs for the given forcing frequency Ω. In terms of the magnitude of the growth rates there are two types of instabilities. The first has relatively high growth rates (exceeding 6×10^{-3}). The growth rate of this type of instability changes only weakly in magnitude as the meridional mode number of the interacting waves is increased. The lowest mode instabilities of this kind are $\{M^-, G_1^+\}$ and $\{M^+, G_1^-\}$. At higher meridional modes, these instabilities correspond to the $\{G_\ell^\mp, G_{\ell+1}^\pm\}$ pairs. Note that all of them are a direct continuation to non-zero k of the additive type instabilities found in d'Orgeville & Hua (2005). Each $k=0$ spike splits in two at non-zero k.

The second set of instabilities has growth rates considerably smaller than those of the first kind, with growth rate decreasing as meridional mode number increases (unlike the instabilities of the first kind). The lower mode instabilities for the second family of spikes are due to a collective excitation of a $\{K, M^+\}$ and an $\{R_1, M^-\}$ pair. Both of these instabilities are of difference type. At higher meridional mode numbers the second family includes $\{R_\ell, G^-_{\ell-1}\}$ and $\{R_\ell, G^+_{\ell+1}\}$ pairs; the first is of a difference type, while the second is of an additive type.

The last column in table 1 shows the growth rates σ_{num} obtained using the Floquet analysis (see figure 1). The growth rates obtained via the method of multiples scales approximate the numerically derived growth rates reasonably well, especially for interactions not involving Rossby waves with meridional mode numbers higher than 1 (σ_{ms} being within less than 1 % of σ_{num}). Rossby waves with higher meridional mode numbers have frequencies comparable to, or even smaller than, the slow time scale. The decrease in accuracy of the method of multiple scales for cases involving these waves is therefore not surprising. The results still agree to within 10 % of accuracy with the numerical calculations, and the method of multiple scales can still be used to interpret the physics of the wave excitation. At higher $\delta\Lambda$ the accuracy of the method of multiple scales for the interactions involving Rossby waves deteriorates even further. However, for interactions that only involve gravity and MRG waves, the method of multiple scales remains very accurate, as long as $\delta\Lambda$ is less than unity.

4. Oscillatory shear combined with a steady shear flow

Here we consider the combination of an oscillatory shear superimposed on a steady background flow. When the steady background flow is stable, one may expect that our analysis from the previous section can be directly carried over with some modest modifications. Although the normal modes are no longer computable analytically, a combination of a multiple-scale approach with a numerical calculation of the coefficients may provide illuminating results. This is a subject of a further study. Here, we confine ourselves exclusively to numerical calculations and concentrate on studying the effects of the oscillatory shear on an 'unstable' steady background flow.

Earlier work on barotropic oscillating shear flows (e.g. Poulin *et al.* 2003) has shown that oscillatory shear tends to stabilize unstable steady background shear flows. In the context of equatorial dynamics, the study of Natarov *et al.* (2008) of a zonally symmetric flow has shown that a small oscillatory shear superimposed on an inertially unstable steady flow also stabilizes the flow to II. At larger values of the oscillatory shear the dominant instability becomes of 'mixed type' (mixed instability, MI), using the terminology of Natarov *et al.* (2008). The MI modes are characterized by the 'parametric sub-harmonic instability' (PSI)-like oscillatory temporal behavior, combined with enhanced 'episodic' growth through an II-like mechanism. In this section we generalize the analysis to three dimensional disturbances.

As an example of the dynamics of a zonally asymmetric case, figure 2 compares the growth rates for an unstable steady shear flow ($\bar{\Lambda} = 2.5$) with and without an oscillating shear (with $\delta\Lambda = 1.0$ for 'small' and $\delta\Lambda = 2.0$ for 'large' magnitude), as functions of k. The background frequency Ω is set to $\sqrt{7}$. Notice that strong instability is confined to zonal wavenumbers $k < 0.4$, i.e. zonal wavelengths substantially larger than the equatorial radius of deformation. The dominant zonal wavenumber $k \approx 0.2$ corresponds to a zonal wavelength five times the Rossby radius of deformation. While at small k ($k < 0.3$) the stabilizing influence of the small oscillatory shear is clear, for higher k the influence is less marked. For high enough k ($k > 0.37$) the oscillation can

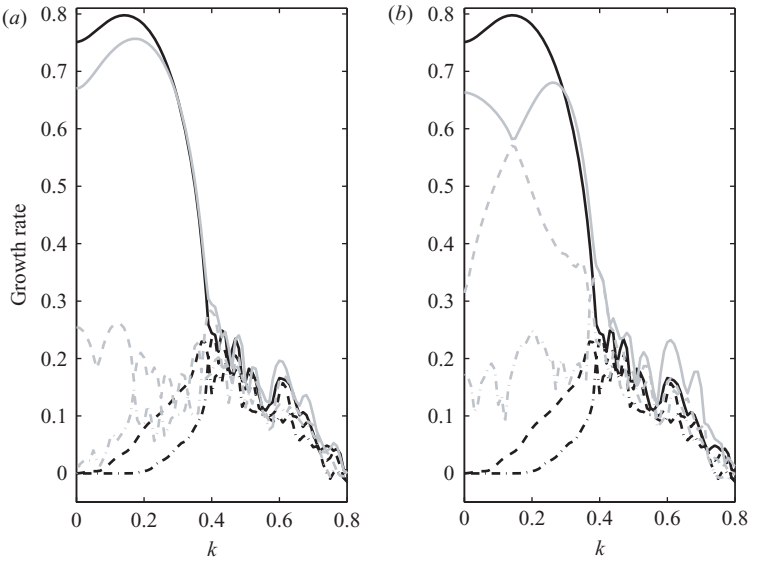

FIGURE 2. Comparison of the growth rate as a function of zonal wavenumber k in a steady shear case $\bar{\Lambda} = 2.5$ (black lines) and a steady shear of the same magnitude combined with an oscillating shear (grey lines) of (*a*) small ($\delta\Lambda = 1.0$) and (*b*) large ($\delta\Lambda = 2.0$) magnitudes. The solid lines correspond to the fastest growing disturbance, and the dashed and dot-dashed lines correspond to the second and third Floquet vectors, respectively.

actually act to promote the instability (figure 2, when the grey curve is higher than the black for a given k).

As for the second and third Floquet vectors, figure 2 shows that they have larger growth rates in the case with oscillatory shear. While there are second and third unstable modes in the steady case, their growth rates are small, especially at small k. The addition of the oscillatory shear introduces the possibility of PSI and MI, with growth rates considerably larger than the growth rate of the second and the third fastest growing modes of the purely steady shear flow (compare the grey and black dashed and dot-dashed curves in figure 2). For the case described here the instabilities that are due to the oscillatory shear are of the mixed type.

As the magnitude of the oscillatory shear $\delta\Lambda$ is increased, the rates associated with the steady-state instability (II and its relatives) continue to drastically diminish at small k but stay about the same magnitude at higher k. The peak of the II mode has shifted from 0.08 at $\delta\Lambda = 1.0$ to 0.12 at $\delta\Lambda = 2.0$. At the same time the MI modes acquire higher growth rates and at some point begin to exceed the growth rate associated with the steady-state instability. At this particular forcing frequency the peak in the MI mode is at $k = 0$. This appears to be the case generally for the MI modes. At smaller $\bar{\Lambda}$ the maximum growth rate induced by the oscillatory shear may shift to asymmetric modes but still with a small k (see next section).

In summary, similar to the zonally symmetric case, the parameter space for zonally asymmetric modes can be separated into regions dominated by PSIs, steady-state instabilities and MIs (see Natarov *et al.* 2008). However, in contrast to the zonally symmetric case, at sufficiently high k oscillatory shear can enhance the growth rates associated with the unstable modes of the steady flow. The oscillatory shear thus provides an additional mechanism for favouring the zonally asymmetric modes. At the same time, at lower k, a moderate oscillatory shear will replace the unstable modes

of the steady shear flow with modes whose temporal behavior resembles that of MIs. In a large part of the parameter space there will co-exist, with similar growth rates, high k modes that are due to the instability of the steady background flow and low-k modes that are excited through MI, both with the same vertical scale.

5. Dominant modes in the continuously stratified ocean

In the previous sections we have been concerned essentially with the inviscid dynamics of a single vertical mode. We will now determine the dominant modes of instability globally in the vertical and zonal wavenumber spaces.

The non-dimensionalization in the previous sections was carried out for a given vertical wavenumber. To look at all vertical modes at once we need to return to the dimensional representation. In this section we solve the problem in a domain that is periodic in the vertical and zonal directions. The height of the domain is set at H and the zonal length at L_x. Because we are using a finite-difference scheme in the meridional direction, the meridional extent of the domain has to be limited. In the meridional direction the domain is centred on the equator and has the half-width of L_y, large enough as not to affect the outcome of calculations. For the purpose of easy comparison with the results, described in Natarov *et al.* (2008), we set the dimensional parameters to the same values as in that paper, including the frequency of the background flow oscillation. The list of parameters is summarized in table 2. Also notice that we now include vertical viscosity.

Figure 3 shows the dominant growth rate and the associated dominant zonal mode number $k^* = kL_x/(2\pi)$ and vertical mode number $m^* = mH/(2\pi)$. Note that we have chosen to present the dominant vertical and zonal modes as pixels at the discrete values of $(\bar{\Lambda}, \delta\Lambda)$ used in the calculations. This form of presentation gives a clearer indication of the rapidly changing dominant modes in the $(\bar{\Lambda}, \delta\Lambda)$ space than a contour plot. The upper panel shows the dominant vertical mode number m^* and is similar in character to the zonally invariant case (see figure 6 of Natarov *et al.* 2008). As before, the regions of small $\bar{\Lambda}$ are dominated by the low-m^* PSIs. The dominant zonal mode number k^*, shown in figure 3(b), however, is high and varies smoothly along the $\bar{\Lambda}$-axis. The dominance of the zonally asymmetric mode can be understood using the results of §3 as follows: In the region around $\delta\Lambda \approx 1.5 \times 10^{-6}\,\mathrm{s}^{-1}$ the dominant vertical mode is $m^* = 8$, and in terms of non-dimensionalized parameters we have $\tilde{\Omega} = \sqrt{8} \approx 2.8$ and

$$\tilde{k} = \frac{2\pi}{100}\frac{k^*}{\sqrt{m^*}} \approx 0.1.$$

The non-dimensionalized $\delta\Lambda$ is approximately 0.2. Figure 1 shows that there are a number of spikes in the vicinity of $\Omega = 2.8$, with the tallest one corresponding to a zonally asymmetric $\{M^+, G_1^-\}$ wave pair.

Large $\bar{\Lambda}$ and small $\delta\Lambda$ are dominated by the high-m^* steady-state instabilities (II and its relatives). It is interesting to note that the physical mechanism of the gravest steady-state instability varies along the $(\delta\Lambda = 0)$-axis in our experiments. Generalizing the parameter E of Taniguchi & Ishiwatari (2006) to a continuously stratified ocean, we introduce the parameter $E_m = \bar{\Lambda}^4/(\beta c_m)^2$. At $\bar{\Lambda} = 1.3 \times 10^{-6}\,\mathrm{s}^{-1}$, the dominant vertical mode corresponds to $m^* = 8$, while at higher $\bar{\Lambda}$ it jumps to $m^* \geqslant 11$. Following Taniguchi & Ishiwatari (2006), we find that for $\bar{\Lambda} = 1.3 \times 10^{-6}\,\mathrm{s}^{-1}$ the parameter $\log E_m$ is equal to $0.43 < 1$. This implies that the dominant instability in this regime is due to the resonance between the equatorial Kelvin modes and

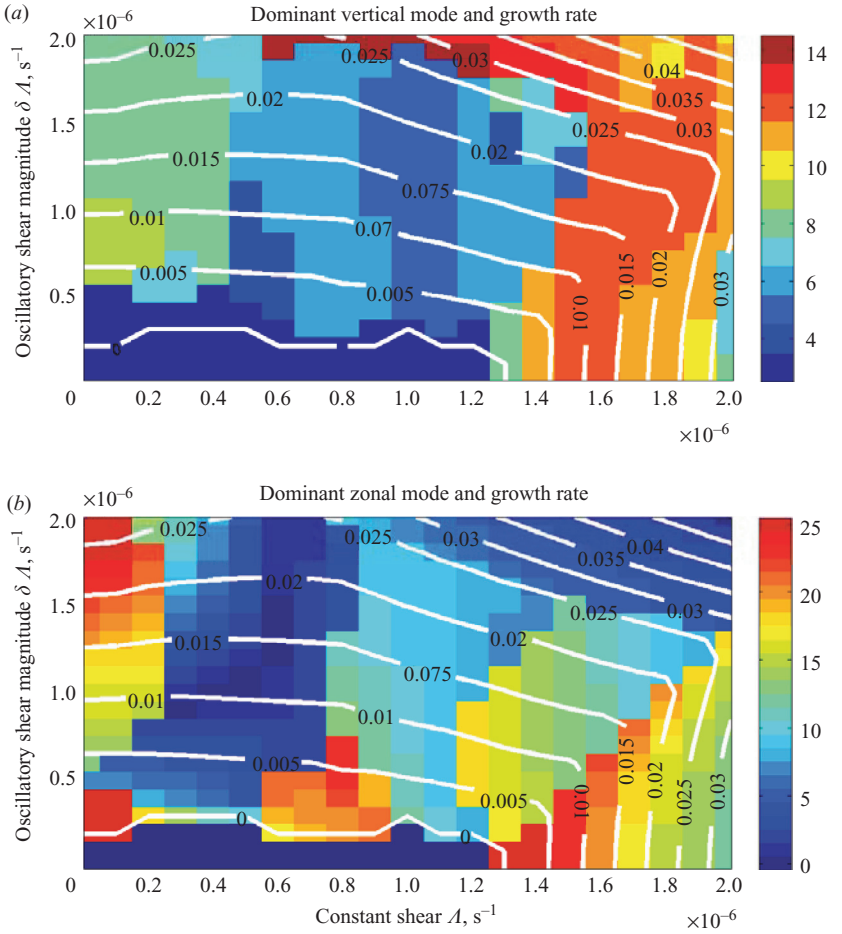

FIGURE 3. Dominant (*a*) m^* and (*b*) k^* modes (colour) and the dominant growth rates (contour) in the dimensional $(\bar{\Lambda}, \delta\Lambda)$-parameter space.

continuous modes (Natarov & Boyd 2001). At higher values of $\bar{\Lambda}$, the parameter $\log E_m$ exceeds 1, and the dominant instabilities are a direct continuation of II to the zonally nonsymmetric case (Dunkerton 1983).

Regardless of the instability mechanism, a small oscillatory shear has a stabilizing influence of the maximum growth rate, similar to the zonally symmetric case and as indicated by the the analysis in § 4. One important difference from the zonally symmetric case is the lack of disparity in dominant vertical scales between steady-state instabilities and MIs. This is a result of the favoured zonal scale. The lower panel of figure 3 shows that the dominant steady-state instabilities are now zonally asymmetric. The dominant zonal mode ranges from $k^* = 25$ at $\bar{\Lambda} = 1.3 \times 10^{-6}\,\mathrm{s}^{-1}$, corresponding to a wavelength of 555 km, to $k^* = 12$ at $\bar{\Lambda} = 2 \times 10^{-6}\,\mathrm{s}^{-1}$, corresponding to a wavelength of 1204 km, and favours a substantially larger vertical scale than the $k^* = 0$ mode.

For larger $\delta\Lambda$ ($>1.5 \times 10^{-6}\,\mathrm{s}^{-1}$) the dominant instabilities are of the mixed type. Figure 3(*b*) shows that MIs still favour zonally symmetric modes (as discussed in § 4), and therefore vertical dominant modes in this region of the parameter space are similar to those found by Natarov *et al.* (2008).

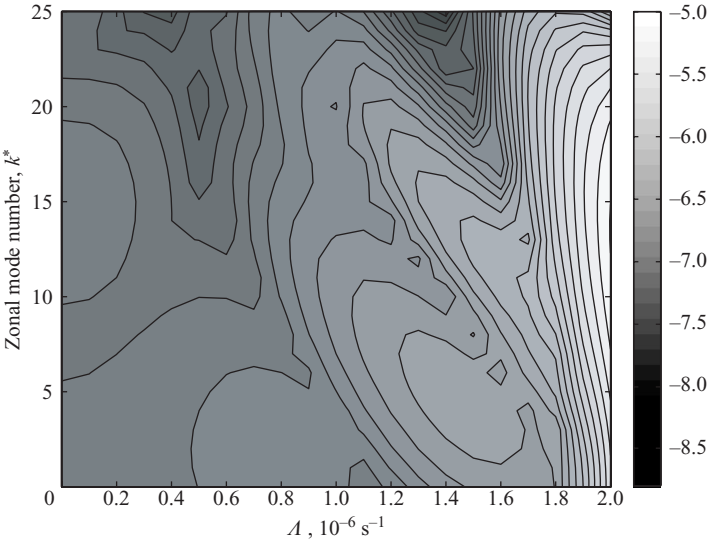

FIGURE 4. Log 2 of the growth rate as a function of $\bar{\Lambda}$ and zonal mode number of the disturbance, k^*, for $\delta\Lambda = 0.8 \times 10^{-6}\,\mathrm{s}^{-1}$.

For smaller values of $\bar{\Lambda}$ the growth rate is relatively flat with respect to k^* but is such that we find the maximum growth rate occurring in bands of high and low k^* as $\bar{\Lambda}$ is varied. Figure 4 shows, as an example, a slice at $\delta\Lambda = 0.8 \times 10^{-6}\,\mathrm{s}^{-1}$ through the $(\bar{\Lambda}, \delta\Lambda, k, m)$ space. As $\bar{\Lambda}$ varies, so does the dominant zonal mode, with relatively sharp transitions at $\bar{\Lambda} = 0.8 \times 10^{-6}\,\mathrm{s}^{-1}$ and $\bar{\Lambda} = 1.4 \times 10^{-6}\,\mathrm{s}^{-1}$. Similar behaviour is found for other values of $\delta\Lambda$. In terms of the vertical scales this region of the parameter space is dominated by the low vertical modes with PSI as the only possible instability mechanism. The alteration of bands is thus due to different zonal modes satisfying the resonance conditions at different values of $\bar{\Lambda}$. The small differences in growth rates between modes indicate that nonlinear effects need to be considered in order to determine the scales that dominate at finite amplitude.

6. Summary and discussion

In this paper, we have addressed the question of the stability of oscillating zonal shear flows on the equatorial β-plane to fully three-dimensional disturbances. For purely oscillatory shear flows (no time-mean shear), we have established, through both numerical Floquet analysis and application of the method of multiple scales, that in addition to the resonant excitation of 'additive' type, described for the zonally symmetric case by d'Orgeville & Hua (2005), resonant excitations of 'difference' type are also possible. We have also described new instabilities, compared to the zonally symmetric case, that are introduced by the existence of Rossby and Kelvin waves in the zonally asymmetric case. These instabilities are especially interesting because they are due to resonances between waves with very different frequencies.

We have established that while oscillatory shear tends to stabilize an unstable steady shear flow for disturbances with a low zonal wavenumber k (similar to many previous studies on oscillatory flows of many sorts), for higher k the effect of oscillatory shear is less significant and may even increase the growth rates. Combining our findings for high and low zonal wavenumbers, we note that a small oscillatory shear tends to push

the dominant zonal wavenumbers to higher values than a purely steady flow with the same time-mean shear. On the other hand, oscillatory shear introduces modes unstable to PSI. As the oscillatory shear is increased, these modes may overtake the steady-state modes at low k and, at some value of $\delta\Lambda$, reach growth rates comparable to those of steady-state instabilities with a high k.

The co-existence, of high- and low-k modes, with similar vertical scale and growth rates but excited through different mechanisms, poses intriguing questions about the nonlinear evolution of the system in this parameter regime. These questions are beyond the scope of the present paper and the subject of future investigation.

An interpretation of our findings in the context of a continuously stratified equatorial ocean model suggests that the stability diagram in the $(\bar{\Lambda}, \delta\Lambda)$-parameter space has a dominant vertical mode structure generally similar to that of a zonally symmetric case. An important difference is in the lack of disparity between the vertical scales selected by steady background state instabilities and MIs. The difference is due to the zonal scale selection. For a wider range of the time-mean shear $\bar{\Lambda}$, the growth rates of different zonal modes are very flat. The rich assortment of vertical and zonal modes we have uncovered for three-dimensional disturbances of zonally symmetric equatorial flows are likely to influence the nonlinear evolution and equilibration of the flow. This again points to nonlinear simulation as the only possible path towards resolving the question of dominant scales.

This work was supported by the NSF under grant number OCE 03-26630 and the Japan Agency for Marine-Earth Science and Technology (JAMSTEC) IPRC/SOEST publication number 574/7605.

Appendix. Calculation of the interaction coefficients γ_{jn}

The meridional structure functions for an equatorial wave j can be found in Ripa (1982) and are given by

$$|j\rangle(y) = \begin{pmatrix} \hat{u}_j(y) \\ \hat{v}_j(y) \\ \hat{\psi}_j(y) \end{pmatrix} = \begin{pmatrix} \mathrm{i}2^{-1/2}\left(b_j^+\varphi_{\ell_j+1} + b_j^-\varphi_{\ell_j-1}\right) \\ b_j\varphi_{\ell_j} \\ \mathrm{i}2^{-1/2}\left(b_j^+\varphi_{\ell_j+1} - b_j^-\varphi_{\ell_j-1}\right) \end{pmatrix}. \tag{A 1}$$

In this expression, φ_ℓ is the normalized Hermite function of order ℓ, and the coefficients b are given by

$$b_K^+ = 1, \quad b_K = 0, \quad b_K^- = 0, \tag{A 2a}$$

$$b_M^+ = \frac{1}{\sqrt{2 - s_M}}, \quad b_M = sgn(\omega_M)\sqrt{1 - s_M}\, b_M^+, \quad b_M^- = 0, \tag{A 2b}$$

$$b_q^\pm = sgn(1 + s_q)\frac{(1 \pm s_q)\sqrt{\ell_q + 1/2 \pm 1/2}}{D_q}, \; b_q = sgn(\omega_q)\frac{\sqrt{(2\ell_q + 1 + s_q)(1 - s_q^2)}}{D_q}, \tag{A 2c}$$

where $M \in \{M^-, M^+\}$ and $q \in \{R_1, G_1^-, G_1^+, \ldots, R_\ell, G_\ell^-, G_\ell^+, \ldots\}$. The quantity $s_j = k/\omega_j$ is the 'zonal slowness' of the wave j and

$$D_q = \sqrt{4\ell_q + 2 + 3s_q - s_q^3}.$$

The spectrum of the equatorial waves consists of a Kelvin wave of frequency

$$\omega_K = k, \quad (s_K = 1, \ell_K = -1), \tag{A 3}$$

eastward and westward MRG waves with frequencies

$$\omega_{M^\pm} = \pm \frac{1}{\sqrt{1 - s_{M^\pm}}}, \quad (|s_{M^\pm}| < 1, \ell_{M^\pm} = 0) \tag{A 4}$$

and Rossby and gravity waves, whose frequencies satisfy

$$\omega_q^2 = \frac{s_q + 2\ell_q + 1}{1 - s_q^2}. \tag{A 5}$$

The zonal slowness of the gravity waves lies in the range $(-1, 1)$, while for the Rossby waves the slowness is always negative.

The operator $\mathscr{H}_1$ is

$$\mathscr{H}_1 = \begin{pmatrix} ky & -\mathrm{i} & 0 \\ 0 & ky & 0 \\ 0 & 0 & ky \end{pmatrix}, \tag{A 6}$$

and the coefficients γ_{jn} are given by

$$\gamma_{jn} = \langle j | \mathscr{H}_1 | n \rangle \equiv \int \mathrm{d}y \cdots = \frac{1}{\sqrt{2}} \left(\delta_{\ell_j, \ell_n - 1} \Gamma^- + \delta_{\ell_j, \ell_n + 1} \Gamma^+ \right), \tag{A 7}$$

where

$$\Gamma^- = -b_n b_j^{+,*} + k \left((\ell_n + 1)^{1/2} b_j^{+,*} b_n^+ + \ell_n^{1/2} b_j^* b_n + (\ell_n - 1)^{1/2} b_j^{-,*} b_n^- \right), \tag{A 8a}$$

$$\Gamma^+ = -b_n b_j^{-,*} + k \left((\ell_n + 2)^{1/2} b_j^{+,*} b_n^+ + (\ell_n + 1)^{1/2} b_j^* b_n + \ell_n^{1/2} b_j^{-,*} b_n^- \right). \tag{A 8b}$$

For the zonally symmetric case $k = 0$ only the first terms in the expressions (A 8) are non-zero.

REFERENCES

Dunkerton, T. J. 1981 On the inertial stability of the equatorial middle atmosphere. *J. Atmos. Sci.* **38**, 2354–2364.

Dunkerton, T. J. 1983 A nonsymmetric equatorial inertial instability. *J. Atmos. Sci.* **40**, 807–813.

Lee, H. & Richards, K. J. 2004 The three-dimensional structure of the interleaving layers in the western equatorial pacific ocean. *Geophys. Res. Lett.* **31**, L07301. Doi:10.1029/2004GL019441.

Natarov, A. & Boyd, J. P. 2001 Beyond-all-orders instability in the equatorial kelvin wave. *Dyn. Atmos. Ocean.* **33**, 191–200.

Natarov, A., Richards, K. J. & McCreary, J. P. 2008 Two-dimensional instabilities of time-dependent zonal flows: linear shear. *J. Fluid Mech.* **599**, 29–50.

d'Orgeville, M. & Hua, B. L. 2005 Equatorial inertial-parametric instability of zonally symmetric oscillating shear flows. *J. Fluid Mech.* **531**, 261–291.

Philander, G. 1990 *El Niño, la Niña, and the Southern Oscillation*. Academic Press.

Poulin, F., Flierl, G. & Pedlosky, J. 2003 The instability of time-dependent shear flows. *J. Fluid Mech.* **481**, 329–353.

Richards, K. J. & Banks, H. 2002 Characteristics of interleaving in the western equatorial pacific. *J. Geophys. Res.* **107** (C12), 3231. Doi:10.1029/2001JC000971.

Ripa, P. 1982 Nonlinear wave-wave interactions in a one-layer reduced-gravity model on the equatorial β plane. *J. Phys. Oceanogr.* **12**, 97–111.

Taniguchi, H. & Ishiwatari, M. 2006 Physical interpretation of unstable modes of a linear shear flow in shallow water on an equatorial beta-plane. *J. Fluid Mech.* **567**, 1–26.